Non-exploding and exploding core-collapse supernova models and the multimessenger predictions

Kei Kotake[1] , Takami Kuroda[2] and Tomoya Takiwaki[3]

[1]Department of Applied Physics & Research Institute of Stellar Explosive Phenomena, Fukuoka University, Jonan, Nanakuma, Fukuoka 814-0180, Japan,

[2]Institute für Kernphysik, Technische Universität Darmstadt, D-64289 Darmstadt, Germany,

[3]Division of Theoretical Astronomy, National Astronomical Observatory of Japan, 2-21-1, Osawa, Mitaka, Tokyo, 181-8588, Japan

Abstract. We present results of full general relativistic (GR), three-dimensional (3D) core-collapse simulation of a massive star with multi-energy neutrino transport. Using a $70 M_\odot$ zero-metallicity star, we show that the black-hole (BH) formation occurs at ~ 300 ms after bounce. At a few ~ 10 ms before the BH formation, we find that the stalled bounce shock is revived by neutrino heating from the forming hot proto-neutron star (PNS), which is aided by vigorous convection behind the shock. Our numerical results present the first evidence to validate the BH formation by the so-called fallback scenario. Furthermore we present results from a rapidly rotating core-collapse model of a $27 M_\odot$ star that is trending towards an explosion. We point out that the correlated neutrino and gravitational-wave signatures, if detected, could provide a smoking-gun evidence of rapid rotation of the newly-born PNS.

Keywords. supernovae:general, hydrodynamics, intabilities, neutrinos, gravitational waves

1. Introduction

Success of direct observations of gravitational waves (GWs) from the compact binary mergers opened a new era of GW astronomy. Up to now, GWs from five binary black hole (BBH) mergers, i.e., GW150914 (Abbott *et al.* (2016)), GW151226 (Abbott *et al.* (2016)), GW170104 (Abbott *et al.* (2017)), GW170608 (Abbott *et al.* (2017)), and GW170814 (Abbott *et al.* (2017)), and one binary neutron star (NS) merger, i.e., GW170817 (Abbott *et al.* (2017)), have been detected by LIGO (Laser Interferometer Gravitational-wave Observatory) Scientific Collaboration and Virgo Collaboration. In the event of GW170817 (Abbott *et al.* (2017)), the electromagnetic-wave counterpart has been detected, which opens yet another new era of multi-messenger astronomy.

One of the most plausible scenarios to explain the BBHs is a binary stellar evolution in a low-metallicity environment (see Abbott *et al.* (2016) for a review). It has been proposed that two massive stars in the approximate range of 40 to $100 M_\odot$ lead to the formation of a massive helium core after experiencing the Roche-lobe overflow and common envelope phase (e.g., Belczynski *et al.* (2010); Langer (2012); Kinugawa *et al.* (2016) for collective references therein). The gravitational collapse of the massive core ($\sim 30 M_\odot$) could account for some of the relevant BH mass ranges (at least in the high-mass end) in the GW events, although the formation path to the massive core and further to the BH is still very uncertain due to the complexity of the binary evolution and the fallback dynamics (e.g., Fryer *et al.* (1999)).

In order to clarify the formation process of the BH, one requires full general relativistic (GR), neutrino radiation-hydrodynamics core-collapse simulations of such massive stars in three-dimensional (3D) space. Due to the high numerical cost, most of the previous studies with BH formation have been done assuming spherical symmetry (1D) (e.g., Janka *et al.* (2016); Kotake *et al.* (2012) and collective references therein). In the context of multi-dimensional (multi-D) simulations with multi-energy neutrino transport, Pan *et al.* (2018) recently reported results from 1D and 2D core-collapse simulations of a solar-metallicity 40 $M_\odot$ star using two-flavor IDSA scheme (Liebendörfer *et al.* (2009)) and a post-Newtonian gravity to include GR effects. A couple of their 2D models showed that the shock revival occurs at ~ 0.7 - 1.2 s after bounce, which is followed by rapid contraction of the proto-neutron star (PNS). More recently, Chan *et al.* (2018) reported a BH-forming 3D-GR simulation of a zero-metallicity 40 $M_\odot$ star with an approximate neutrino transport (FMT) scheme. Thus far the BH formation has not yet been explored in the context of 3D simulations with detailed neutrino transport schemes in GR as proposed in Shibata *et al.* (2011).

In this contribution, we primarily present results of the BH forming, 3D-GR simulations of a $70 M_\odot$ star based on our recent work (Kuroda *et al.* (2018)). We start to briefly summarize our numerical method for GR-radiation hydrodynamics and initial models in Section 2. Section 3 summarizes the results, in which we also present our recent outcomes from exploding 27 $M_\odot$ star based on Takiwaki and Kotake (2018).

2. Numerical method and initial models

In our full GR radiation-hydrodynamics simulations, the evolution equations of metric, hydrodynamics are solved based on the BSSN formalism (Shibata & Nakamura (1995); Baumgarte and Shapiro (1999)) and the evolution of neutrino radiation field based on the multi-energy M1 scheme (Kuroda *et al.* (2018)).

We use a zero-metallicity $70 M_\odot$ star of Takahashi *et al.* (2014), which we refer to as Z70 below. At the precollapse phase of Z70, the mass of the central iron core is $\sim 2.8 M_\odot$ and the enclosed mass up to the helium layer is $\sim 31 M_\odot$. For comparing with previous results, we also compute a solar-metallicity $40 M_\odot$ star of Woosley *et al.* (2002) that we refer to as S40. Note that the compactness parameter of S40 is much smaller ($\xi_{2.5} \sim 0.26$) than that of Z70.

We use the equation of state (EOS) by Lattimer & Swesty (1991) with a bulk incompressibility modulus of $K = 220$ MeV (LS220). The 3D computational domain is a cubic box with 15,000 km width, and nested boxes with nine refinement levels are embedded in the Cartesian coordinates. Each box contains 64^3 cells, and the minimum grid size near the origin is $\Delta x = 458$m. Throughout this contribution, $T_{\rm pb}$ denotes the time after bounce.

Extraction of GWs is done by the conventional quadrupole formula (Misner *et al.* (1973)), in which the transverse and the traceless gravitational field h_{ij} is expressed as,

$$h_{ij}(\theta, \phi) = \frac{A_+(\theta, \phi)e_+ + A_\times(\theta, \phi)e_\times}{D}. \tag{2.1}$$

In Eq.(2.1), $A_{+/\times}(\theta, \phi)$ represent the amplitude of orthogonally polarized wave components with emission angle (θ, ϕ) dependence, $e_{+/\times}$ denote unit polarization tensors and D is the source distance where we set $D = 10$ kpc in this contribution, unless otherwise stated.

3. BH forming simulation of a 70 $M_\odot$ Star

3.1. *3D hydrodynamics up to the BH formation*

The top panel of Fig. 1 shows temporal evolution of the maximum density $\rho_{\rm max}$ (solid lines) and the minimum lapse $\alpha_{\rm min}$ (dotted lines) for Z70 (red line) and S40 (black line),
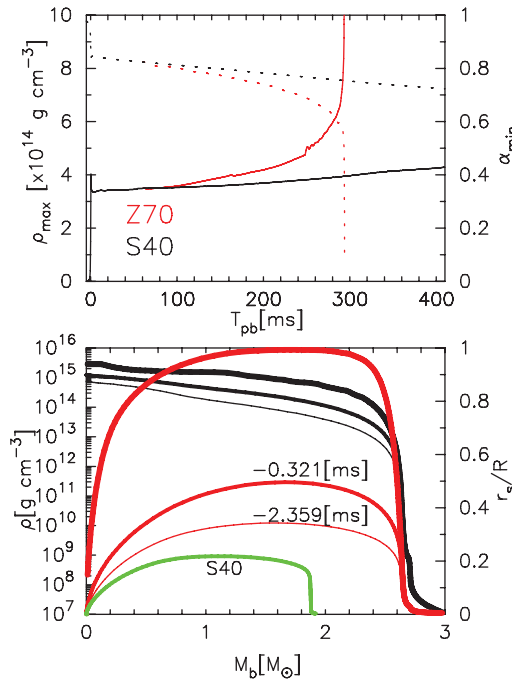
Figure 1. The top panel shows time evolution of the maximum rest-mass density (solid line) and minimum lapse function (dotted line) for Z70 (red line) and S40 (black line), respectively. The bottom panel shows angle-averaged profiles of the (rest-mass) density (black line) and the ratio r_s/R (red lines, see text) for Z70 as a function of the enclosed baryon mass for three representative time slices near the final simulation time. "-0.321" and "-2.359" ms denote the time before the final simulation time ($T_{\rm fin} = 293$ ms after bounce). The green line corresponds to r_s/R for S40. These figures are from Kuroda *et al.* (2018).

respectively. The maximum density at bounce ($\rho_{\rm max} \sim 4 \times 10^{14}$ g cm^{-3}) is quite similar between Z70 and S40. After bounce, the increase of the maximum density of Z70 (red solid line) is significantly faster than that of S40 (black solid line). In Z70, we terminated the computation at $T_{\rm fin} = 293$ ms after bounce because it exceeds the (temperature) range of the EOS table used in our simulation. In both Z70 and S40, the minimum lapse (dotted lines) shows a gradual decrease after bounce. At around $T_{\rm fin}$, it shows a drastic drop to $\alpha_{\rm min} = 0.0645$ for Z70, indicating that the PNS core starts to collapse rapidly toward a BH formation.

The bottom panel of Fig. 1 explains how $T_{\rm fin}$ is related to the BH formation time. We show the profiles of (angle-averaged) density (black lines) and a diagnostics to measure the BH formation as a function of the enclosed baryon mass M_b at some representative snapshots near $T_{\rm fin}$ for Z70 (red lines) and at $T_{\rm pb} = 400$ ms for S40 (green line). We estimate the diagnostics by the ratio r_s/R where r_s and R is the Schwarzschild radius and the radial coordinate, respectively. One can see that the maximum r_s/R is ~ 0.3 at 2.359 ms before $T_{\rm fin}$ (the thin red line labelled by "-2.359 [ms]") and rapidly increases with time, approaching to unity (precisely, 0.932) at $T_{\rm fin}$ (thickest red line), which we judge as the epoch of the BH formation in this work.

At the (fiducial) BH formation time, the mass and the radius is $M_{b(g),BH} \sim 2.60(2.51)$ $M_\odot$ and $R_{\rm iso} \sim 4$ km, respectively (see the thickest red line in the bottom panel of Fig. 1). By contrast, S40 shows significantly less compact structure (green line) at the final simulation time ($T_{\rm pb} = 400$ ms). The BH formation should occur much later, possibly when the mass shell at $R(M_b = 2.6 M_\odot) \sim 10^9$ cm accretes to the stalled shock. Using the same
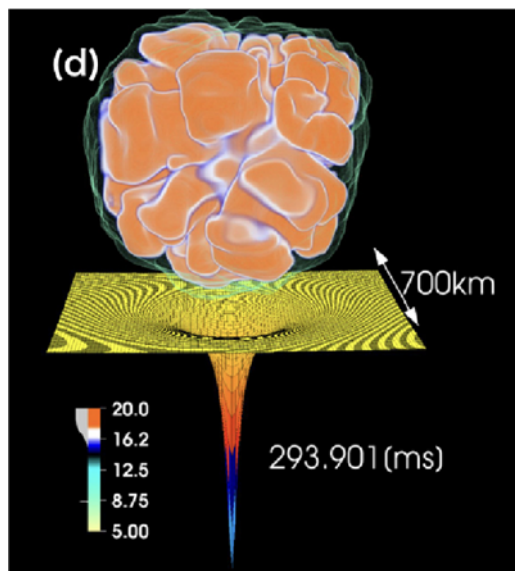
Figure 2. A snapshot of the entropy distribution (k_B baryon^{-1}) for Z70 at $T_{pb} \sim 294$ ms just before the BH formation (Kuroda *et al.* (2018)). The sheet represents the lapse function (α) on the $z = 0$ plane.

EOS (LS220), this expectation is in line with Pan *et al.* (2018) who reported the BH formation at $T_{pb} \sim 700$ ms and with Chan *et al.* (2018) at $T_{pb} \sim 1$ s.

The time evolution of the (angle-averaged) shock radii R_s, the gain radius R_g, the ratio of the advection timescale to the neutrino-heating timescale in the gain region τ_{adv}/τ_{heat} (e.g., Buras *et al.* (2006); Kuroda *et al.* (2012)), and the mass in the gain region M_{gain} is presented in Figure 2 of Kuroda *et al.* (2018), respectively. For model Z70, the shock revival was obtained after $T_{pb} \gtrsim 260$ ms. At this time, the maximum temperature in the core becomes as high as $T \sim 100$ MeV at a slightly off-center region at $R_{iso} \sim 10$ km (equivalently at $M_b \sim 1.0\ M_\odot$). Subsequently the high temperature region propagates outward in the mass coordinate, although spatially inward, due to the continuous mass accretion. The maximum temperature reaches ~ 170 MeV at $R_{iso} \sim 1$ km ($M_b \sim 1.4\ M_\odot$) just before T_{fin}. In this second collapse phase to the forming BH, the high neutrino emission makes the heating timescale shorter than the competing advection timescale in the gain region. Aided by strong convection behind the shock, the stalled shock is revived at $T_{pb} \gtrsim 260$ ms ($\tau_{adv}/\tau_{heat} \geqslant 1$). This also results in the increase in the gain mass (see the blue line) due to the shock expansion.

Fig. 2 visualizes the 3D hydrodynamics feature near at the BH formation. During the first ~ 160 ms after bounce, the neutrino heating is still weak and high entropy bubbles are yet to appear. After $T_{pb} \gtrsim 230$ ms, the formation of high entropy plumes ($s \gtrsim 15k_B$ baryon^{-1}) can be seen. At this time, the mass in the gain region M_{gain} also starts to increase. The expansion of the (merging) high entropy plumes is clearly seen, leading to the shock revival. The lapse function shows a steepest drop in the center (see the cusp in the plane), which corresponds to the BH formation. By expanding the shock radius into the spherical harmonics, we find that the deviation of the shock from spherical symmetry (in the low-modes $\ell = 1, 2$) is less than $\sim 2\ \%$. This clearly indicates that neutrino-driven convection dominates over the SASI (standing accretion shock instability, Foglizzo *et al.* (2015)) in this case.
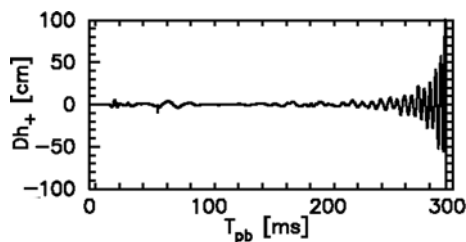
Figure 3. Gravitational waveform for Z70. Note that h_+ and D denote the GW amplitude of the + polarization and the distance to the source, respectively.

Finally, we show in Fig. 3 the gravitational waveform for Z70. The waveform is extracted along positive z-axis via the quadrupole formula. The GW amplitude stays at small value $Dh \lesssim 10$ cm before the shock expansion occurs ($T_{\mathrm{pb}} \sim 260$ ms). The strong GW emission thereafter mainly originates from strong convection motion behind the shock. Just before the final simulation time, the GW amplitude reaches ~ 100 cm. The detection horizon of this signal reaches ~ 1 Mpc for the third-generation GW detectors such as the Einstein Telescope (ET) and the Cosmic Explorer (CE) (Hild *et al.* (2011); Abbott *et al.* (2017)). Regarding the neutrino luminosity and rms energy, both electron type (anti-)neutrinos show decreasing and plateau trend for $T_{\mathrm{pb}} \gtrsim 260$ ms, respectively. On the other hand, heavy-lepton neutrinos show a rapid increase both in the luminosity and rms energy. As previously identified in 1D full-GR simulations with Boltzmann neutrino transport (Liebendörfer *et al.* (2004)), these features are commonly observed in the literature that is due to rapid contraction of the PNS to the forming BH (see also, Sumiyoshi *et al.* (2007); Fischer *et al.* (2014)). The detection of the short-live (~ 300 ms after bounce) neutrino signals are basically limited to Galactic events (see Mirizzi *et al.* (2016) for a review). However, further study would be needed to clarify the contribution of these BH forming massive stars to the prediction of diffuse neutrino supernova background (e.g., Lunardini (2009); Horiuchi *et al.* (2018)).

3.2. *Neutrino and GW signals from an exploding* $27 M_\odot$ *star*

Figure 4 shows the neutrino and GW signals (Takiwaki and Kotake (2018)) obtained in 3D core-collapse supernova simulation of a rapidly rotating 27 $M_\odot$ star that is exploding due to the growth of the so-called low-T/$|W|$ instability (Takiwaki *et al.* (2016)). The time modulation seen in the left panel corresponds to the neutrino light-house effect where the spinning of strong neutrino emission regions around the rotational axis leads to quasi-periodic modulation in the neutrino signal. Depending on the observer's viewing angle, the time modulation will be clearly detectable in IceCube and the future Hyper-Kamiokande. The GW emission is also anisotropic where the GW signal is emitted, as previously identified (see Kotake (2013) for a review), most strongly toward the equator at rotating core-collapse and bounce, and the non-axisymmetric instabilities in the postbounce phase lead to stronger GW emission toward the spin axis. The right panel in Figure 4 shows that these GW signals can be a target of LIGO-class detectors for a Galactic event. The origin of the postbounce GW emission naturally explains why the peak GW frequency is about twice of the neutrino modulation frequency. We point out that the simultaneous detection of the rotation-induced neutrino and GW signatures could provide a smoking-gun signature of a rapidly rotating PNS at the birth.
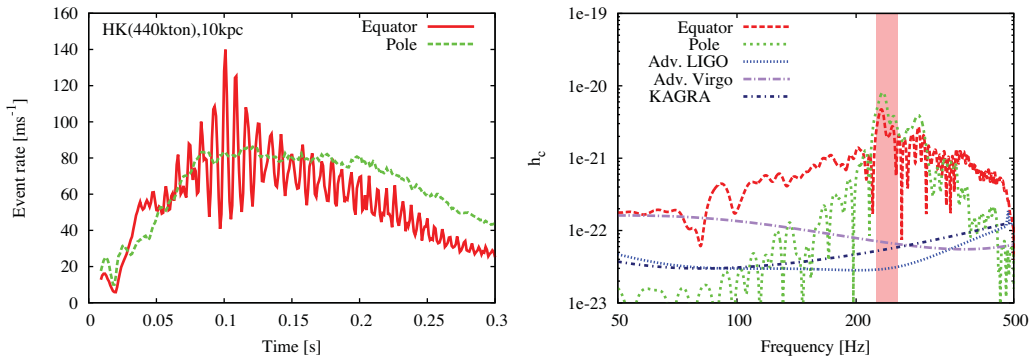
Figure 4. The left panel shows detection rates of $\bar{\nu}_e$ at 10 kpc for our rapidly rotating $27M_\odot$ model as a function of time after bounce (Takiwaki and Kotake (2018)). The red and green lines correspond to the event rates (per 1 ms bin) for an observer along the equator and the pole, respectively. A quasi-periodic modulation of ~ 200 Hz (red lines) is clearly seen for the observer along the equator. The right panel shows the characteristic GW spectra relative to the sensitivity curves of advanced LIGO, advanced Virgo (Hild *et al.* (2009)) and KAGRA (Aso *et al.* (2013)). Note that in the right plot, we focus on only the frequency range ($\lesssim 500$ Hz) with the maximum sensitivity.

4. Perspectives

First we need to investigate the dependence of numerical resolution on the presented results (Melson *et al.* (2020); Nagakura *et al.* (2019)). For enhancing predictive power of the multi-messenger predictions, we also need to implement more detailed neutrino opacities as in Kotake *et al.* (2018). Detailed analysis of GW polarization from rapidly rotating $27\ M_\odot$ should deserve further investigation (Hayama *et al.* (2018); Kawahara *et al.* (2018)). We have only presented a snapshot of our continuing endeavor for making more precise multi-messenger predictions based on more sophisticated 3D-GR models.

Acknowledgment

References

Abbott, B. P. *et al.* 2016, (LIGO Scientific Collaboration and Virgo Collaboration), *Phys. Rev. Lett.* 116, 061102
Abbott, B. P. *et al.* 2016, (LIGO Scientific Collaboration and Virgo Collaboration), *Phys. Rev. Lett.* 116, 241103
Abbott, B. P. *et al.* 2017, (LIGO Scientific Collaboration and Virgo Collaboration), *Phys. Rev. Lett.* 118, 221101
Abbott, B. P., Abbott, R., Abbott, T. D., *et al.* 2016, *ApJ*, 818, L22
Abbott, B. P. *et al.* 2017, (LIGO Scientific Collaboration and Virgo Collaboration), *Astrophys. J.* 851, L35
Abbott, B. P. *et al.* 2017, (LIGO Scientific Collaboration and Virgo Collaboration), *Phys. Rev. Lett.* 119, 141101
Abbott, B. P. *et al.* 2017, (LIGO Scientific Collaboration and Virgo Collaboration), *Phys. Rev. Lett.* 119, 161101

Abbott, B. P. *et al.* 2017, (LIGO Scientific Collaboration and Virgo Collaboration), *ApJ* 848, L12

Abbott, B. P. *et al.* 2017, *Classical and Quantum Gravity*, 34, 044001

Andresen, H., Müller, B., Müller, E., Janka, H.-Th. 2017, *MNRAS*, 468, 2032

Aso, Y., Michimura, Y., Somiya, K., *et al.* 2013, *Phys. Rev. D*, 88, 043007

Baumgarte, T. W. & Shapiro, S. L. 1999, *Phys. Rev. D*, 59, 024007

Belczynski, K., Dominik, M., Bulik, T., *et al.* 2010, *ApJ*, 715, L138

Buras, R., Janka, H.-T., Rampp, M., & Kifonidis, K. 2006, *A&A*, 457, 281

Chan, C., Müller, B., Heger, A., Pakmor, R., & Springel, V. 2018, *ApJ*, 852, L19

Fischer, T., Hempel, M., *et al.* 2014, *European Physical Journal A*, 50, 46

Foglizzo, T., Kazeroni, R., Guilet, J., *et al.* 2015, *PASA*, 32, e009

Fryer, C. L., Woosley, S. E., & Hartmann, D. H. 1999, *ApJ*, 526, 152

Hayama, K., Kuroda, T., Kotake, K., & Takiwaki, T. 2018, *MNRAS*, 477, L96

Hild, S., Freise, A., Mantovani, M., *et al.* 2009, *Classical and Quantum Gravity*, 26, 025005

Hild, S., Abernathy, M., Acernese, F., *et al.* 2011, *Classical and Quantum Gravity*, 28, 094013

Horiuchi, S., Sumiyoshi, K., Nakamura, K., *et al.* 2018, *MNRAS*, 475, 1363

Janka, H.-T., Melson, T., & Summa, A. 2016, *Annual Review of Nuclear and Particle Science*, 66, 341

Kawahara, H., Kuroda, T., Takiwaki, T., Hayama, K., & Kotake, K. 2018, *ApJ*, 867, 126

Kinugawa, T., Nakano, H., & Nakamura, T. 2016, *Progress of Theoretical and Experimental Physics*, 2016, 103E01

Kotake, K., Sumiyoshi, K., Yamada, S., *et al.* 2012, *Progress of Theoretical and Experimental Physics*, 2012, 01A301

Kotake, K. 2013, *Comptes Rendus Physique*, 14, 318

Kotake, K., Takiwaki, T., Fischer, T., Nakamura, K., & Martínez-Pinedo, G. 2018, *ApJ*, 853, 170

Kuroda, T., Kotake, K., & Takiwaki, T. 2012, *ApJ*, 755, 11

Kuroda, T., Kotake, K., Takiwaki, T., & Thielemann, F.-K. 2018, *MNRAS*, 477, L80

Langer, N. 2012, *ARA&A*, 50, 107

Liebendörfer, M., Messer, O. E. B., Mezzacappa, A., *et al.* 2004, *ApJS*, 150, 263

Liebendörfer, M., Whitehouse, S. C., & Fischer, T. 2009, *ApJ*, 698, 1174

Lunardini, C. 2009, *Phys. Rev. Lett.*, 102, 231101

Melson, T., Kress, D., & Janka, H.-T. 2020, *ApJ*, 891, 1

Misner, C. W., Thorne, K. S., & Wheeler, J. A. 1973, Gravitation

Mirizzi, A., Tamborra, I., Janka, H.-T., *et al.* 2016, *Nuovo Cimento Rivista Serie*, 39, 1

Müller, B., Janka, H.-T., & Marek, A. 2013, *ApJ*, 766, 43

Murphy, J. W., Ott, C. D., & Burrows, A. 2009, *ApJ*, 707, 1173

Nagakura, H., Burrows, A., Radice, D., Vartanyan, D., *et al.* 2019, *MNRAS*, 490, 4622

Pan, K.-C., Liebendörfer, M., Couch, S. M., & Thielemann, F.-K. 2018, *ApJ*, 857, 13

Shibata, M. & Nakamura, T. 1995, *Phys. Rev. D*, 52, 5428

Shibata, M., Kiuchi, K., Sekiguchi, Y., & Suwa, Y. 2011, *Progress of Theoretical Physics*, 125, 1255

Sumiyoshi, K., Yamada, S., & Suzuki, H. 2007, *ApJ*, 667, 382

Takiwaki, T. & Kotake, K. 2018, *MNRAS* 475, L91

Takiwaki, T., Kotake, K., & Suwa, Y. 2016, *MNRAS*, 461, L112

Takahashi, K., Umeda, H., & Yoshida, T. 2014, *ApJ*, 794, 40

Woosley, S. E., Heger, A., & Weaver, T. A. 2002, *Reviews of Modern Physics*, 74, 1015